Experimental Study of Sour Top-of-the-Line Corrosion Using a Novel Experimental Setup

M. Singer,[‡,] J. Al-Khamis,[**] and S. Nešić[*]*

ABSTRACT

Top-of-the-line corrosion (TLC) is a potential issue for carbon steel pipelines transporting natural gas. This type of corrosion is driven mostly by the gradient of temperature between the warm produced fluids and the outside environment, but also is affected strongly by the presence of corrosive species such as carbon dioxide (CO_2), hydrogen sulfide (H_2S), and organic acids. This paper presents an assessment of the corrosion risk of a specific sour offshore development: the Karan gas field (Arabian Gulf, Saudia Arabia). The study was performed through laboratory experiments in a large-scale flow loop as well as in a specially designed autoclave equipped for corrosion studies under dewing conditions. Corrosion rates were obtained using the weight-loss method and the surface layer was analyzed with x-ray diffraction (XRD), energy-dispersive spectroscopy (EDS), and scanning electron microscopy (SEM). The TLC rate was found to be low under all conditions tested, and no indications of localized corrosion were observed. Mackinawite, cubic iron sulfide, and troilite (stoichiometric pyrrhotite) were identified in the corrosion product layer.

KEYWORDS: carbon dioxide, hydrogen sulfide, top-of-the-line corrosion, water condensation rate

INTRODUCTION

The Karan gas field (Arabian Gulf, Saudia Arabia) initially will be comprised of four wellhead production platforms, each functioning unmanned to receive, commingle, and export up to 14 $MMSm^3/d$ of gas from a number of production wells to one central tie-in platform (TP) via 0.51 m diameter flowlines (1.1 km to 7 km in length). A single, 0.96 m internal diameter (ID), 110 km trunk line will transport the wet produced gas from the TP to the onshore gas processing facility. Of the 110 km, 85 km are offshore, and the remaining 25 km are onshore. The gas is lean, with no hydrocarbon condensate dropping out in the planned operational region. The presence of carbon dioxide (CO_2; 8 mol%) and hydrogen sulfide (H_2S; 4 mol%) should lead to aggressive corrosion environments.

In offshore wet sour gas production with long pipelines, hydrate and corrosion inhibition is required to ensure safe, reliable, and cost-effective operations. With the identified operating conditions, corrosion will be a major concern for the operation of the Karan facilities. Identifying the nature of the anticipated corrosion processes is the key to determining the major components of any future corrosion management program. In particular, top-of-the-line corrosion (TLC) is identified as a potential issue in specific locations in the field, since large quantities of organic acids are present in the condensed water.

TLC is a type of corrosion that happens in stratified flow when strong gradients of temperature between the outside environment and the process fluid lead to water condensation on the internal walls of the pipeline. It was first identified in the 1960s,[1] but many field cases, both for onshore and offshore production environments, have been published since then.[2-8] This type of corrosion occurs due to the pres-

Submitted for publication: May 11, 2012. Revised and accepted: January 10, 2013. Preprint available online: February 5, 2013, http://dx.doi.org/10.5006/0738E.

‡ Corresponding author. E-mail: singer@ohio.edu.
* Institute for Corrosion and Multiphase Technology, Ohio University, 342 West State St., Athens, OH 45701.
** Saudi Arbian Oil Company, Consulting Services, Dhahran, Saudi Arabia.

ISSN 0010-9312 (print), 1938-159X (online)
13/000115/$5.00+$0.50/0 © 2013, NACE International

ence of condensed water and leads to severe pitting and uniform corrosion on the upper part of the pipe (between the 9 and 3 o'clock positions).

There are two different categories of TLC depending on whether TLC is dominated by CO_2 or H_2S. TLC in sweet (CO_2) conditions depends mostly on the water condensation rate (WCR), the gas temperature, the gas flow rate, the CO_2 partial pressure, and the presence of organic acid. Initiation of localized corrosion is associated with breakdowns of an otherwise protective iron(II) carbonate ($FeCO_3$) layer. Small pits grow in depth and width and eventually coalesce, leading to more uniform-like corrosion over extended areas of the top of the pipeline.[9-14]

In sour environments, the basic principle still holds that corrosion occurs as a result of the presence of condensed water at the metal surface. However, the specifics of the corrosion mechanism can be quite different compared to a CO_2-dominated environment. There is only a limited amount of work that has been published so far on sour TLC.[15-17] Sour TLC field cases are quite rare, but some field failures have been reported.[1,4-8] It seems that the controlling parameters are related to the protectiveness of the corrosion product layer, which should be mostly dependent on the fluid temperature, pH, and iron ion content.

Extensive experimental work performed for multiphase, bottom-of-the-line conditions has shown a reduction of the corrosion rate compared to a baseline pure CO_2 environment when small amounts of H_2S are introduced.[18-21] This is associated with the formation of a protective mackinawite film. However, various thermodynamically stable types of iron(II) sulfide (FeS) have been reported,[22] and this could lead to widely different corrosion behaviors, linking FeS phase to protectiveness characteristics. Finally, the presence of organic acids, identified as a key parameter in sweet environments,[9] also could play a role in sour TLC. This has been reported to affect the protectiveness of mackinawite greatly and lead to localized corrosion in bottom-of-the-line corrosion.[23]

OBJECTIVES

The objective of this work was to simulate as closely as possible the environment of the Karan sour gas field to evaluate the likelihood of TLC and to collect useful information about general and localized TLC rates. The thermo-hydrodynamics and the chemistry of the field conditions have to be matched closely. While large-scale loops are fully equipped for realistic TLC investigation, they are limited in terms of H_2S content because of the safety concerns associated with the presence of large quantities of toxic gas. On the other hand, autoclaves have been used successfully to conduct high-pressure H_2S corrosion tests even if they cannot reproduce the hydrodynamics encountered in a gas pipeline. By combining tests performed in large-scale loops and in autoclaves, it is believed that the different aspects of the wet gas field case may be investigated closely. Each test was carried out for 3 weeks and a variety of corrosion monitoring techniques were used to quantify the extent of TLC. A summary of the range of conditions tested is displayed in Table 1.

TABLE 1
Large-Scale Flow Loop vs. Autoclave

Large-scale loop tests:
Total pressure: 300 kPa
H_2S partial pressure: up to 10 kPa
CO_2 partial pressure: up to 50 kPa
CO_2/H_2S ratio: up to 5
Flow regime: Stratified flow (gas velocity: 5 m/s)
Autoclave tests:
Total pressure: 5,000 kPa
H_2S partial pressure: up to 400 kPa
CO_2 partial pressure: up to 1,000 kPa
CO_2/H_2S ratio: up to 5
Flow regime: Stagnant conditions

TEST MATRIX

Table 2 presents the detailed conditions under which the flow loop tests were performed. Although the thermo-hydrodynamic effect was properly simulated, only the H_2S/CO_2 ratio was similar to the field conditions (not the actual partial pressures). The organic acid used was HAc (acetic acid).

Table 3 presents the experimental conditions of the large-scale (20 L) autoclave tests (made from UNS N10276[1]). The objective of Test 3 was to build a link between autoclave and flow loop tests. Tests 4 through 7 more closely represent the wet gas field conditions (H_2S and CO_2 partial pressures).

EXPERIMENTAL PROCEDURES

Large-Scale Flow Loop

The first two experiments were carried out in a UNS N10276 0.1 m ID flow loop, under a multiphase stratified flow of water and a mixture of CO_2/H_2S. A complete description of the procedure followed during the experimental part can be found elsewhere,[15] but some key aspects of the experimental method are discussed below.

The flow loop setup can be divided into three main parts: the tank, the pump and the piping.

—The tank was used for the liquid phase conditioning and heating. It was filled with deionized water. A set of immersion heaters controlled the temperature.

[1] UNS numbers are listed in *Metals and Alloys in the Unified Numbering System*, published by the Society of Automotive Engineers (SAE International) and cosponsored by ASTM International.

TABLE 2
Tests 1 and 2—Large-Scale Flow Loop Tests—Experimental Conditions

Parameters	Test 1		Test 2
Absolute pressure (kPa)		300	
pCO_2 (kPa)		50	
Gas temperature (°C)		55	
Water condensation rate (WCR) (mL/m^2/s)	0.25		0.05
Gas velocity (m/s)		5	
Undissociated HAc in tank (mg/L)	250		350
H_2S partial pressure (kPa)		10	
Steel type (coupons)		API X65	
pH (tank)		As measured (4.2)	
Test duration (weeks)		3 weeks	

TABLE 3
Tests 3 through 7—Large-Scale (20 L) Autoclave—Experimental Conditions

Parameters	Test 3	Test 4	Test 5	Test 6	Test 7
Gas temperature (°C)	39.3	45.5	55	55	
Steel temperature (°C)	17	38.1	21.4	50	24.4
Absolute pressure (kPa)	220	2,620	2,690	28.4	
pH_2S (kPa)	110	199	124	4.29	
pCO_2 (kPa)	41	813	940	9.9	
CO_2/H_2S ratio	3.7	4.1	7.6	2.3	
Undissociated HAc (mg/L)			350		
WCR (mL/m^2/s)	0.14	0.02	0.12	0.02	0.14

—Positive displacement progressive cavity pumps and gas blowers were used to move the liquid and the gas.

—The 0.1 m ID flow piping (in the form of a closed loop) was 30 m long and horizontally level.

At the beginning of the experiment, 1,000 L of deionized water was introduced in the tank. The system then was heated and pressurized with the required partial pressure of CO_2. A set of thermocouples located at different points along the flow loop were used to monitor the liquid and gas temperature. The gas flow rate was controlled directly by the gas pump frequency (no gas flow meter is installed in the system). The gas pump was a positive displacement pump that required a minimum amount of liquid water for lubrication. This water was carried along the loop together with the gas but remained clearly stratified and no droplet entrainment or annular flow regime was expected.

Once the conditions were stable, the pH of the bulk liquid phase was measured and a controlled amount of glacial acetic acid was injected into the tank under pressure. Being a weak acid, it partially dissociated in the water and formed acetate ions and protons, slightly decreasing the pH of the aqueous solution. The volume of acetic acid initially injected was calculated based on the temperature and bulk pH and set so that the undissociated acetic acid concentration specified in the test matrix was reached. There was no simple way to monitor potential changes in undissociated acetic acid concentration during the test. Instead, the bulk pH was controlled at a fixed value (by adding hydrochloric acid [HCl]) to ensure that the chemistry remained globally unchanged. As long as the bulk pH remained constant, there was no reason to suspect that the test conditions should vary in this closed system. At the end of the test, a liquid sample was taken from the tank and analyzed through ion chromatography. The vapor pressure of acetic acid was directly dependent on the undissociated acetic acid concentration in the aqueous phase and on the temperature. It was calculated using Henry's law, but was never measured directly during the experiments.

The test section, where the corrosion measurements were taken, was located 8 m downstream of a straight pipe section. The test section (Figure 1) was comprised of a 1.5 m long pipe spool piece and had four probe ports (two at the top, two at the bottom). The steel samples had a diameter of 5.7 cm and were made of API X65 steel. The whole surface of the steel samples was coated with an electrical insulator except for the "face" exposed to the flowing gas phase. Prior to each test, the samples were polished using 600 grit sand paper and cleaned with isopropanol (C_3H_8O).

Tap water was circulated through a set of cooling coils wrapped around the pipe, effectively cooling the pipe wall and consequently the corrosion samples. The temperature of the steel surface was measured using a specially designed temperature probe. The vapor condensed on the pipe wall but its rate was not measured directly. Instead, an in-house model was used to calculate the water condensation rate. This model has been developed considering heat/mass transfer theory applied to dropwise condensation and

has been calibrated carefully through a number of flow loop experiments. The reader is invited to review the original publication[24] for more details.

Autoclave

The autoclave tests were conducted in a 20 L autoclave made of UNS N10276. The autoclave was specially manufactured to enable corrosion measurements under condensing conditions. The top lid of the autoclave was equipped with an internal cooling system and the sample holder plate (Figure 2). The steel samples were made of API X65 steel and prepared the same way as for the flow loop tests. The design of the sample holder enabled study of the effect of the various condensation rates in one single test. This was done by "hanging" some of the steel samples in the gas phase but away from the cooled plate, experiencing much less condensation. The samples were not immersed in the bulk liquid phase.

Eight liters of deionized water was introduced in the autoclave at the beginning of the test and deoxygenated for 2 h before the correct amount of pure acetic acid could be introduced.

The sample holder was then attached to the top lid and the autoclave was sealed, heated to the required temperature, and pressurized with N_2 to 200 kPa total pressure. Pure H_2S gas then was bubbled into the fluid until the total pressure reached a stable required reading (200 or 400 kPa of H_2S). In the same manner, CO_2 was added to reach a partial pressure of 1,000 kPa, and the pressure was increased up to 2,500 kPa with N_2. The concentration of H_2S in the gas phase was measured at the end of the test using colorimetric gas detector tubes. According to calculation, the pH of the main liquid bulk solution should have remained around pH 3.4 to 3.5 during the 3 weeks of testing. The temperature of the steel sample holder was measured using a thermocouple, and the water condensation was calculated using the same in-house heat/mass-transfer model developed for the flow loop test. At the end of the test, the gas phase was purged for a few hours with nitrogen before opening the autoclave and removing the steel samples. A liquid sample then was taken for acetic acid analysis. The steel samples were dried and weighed. X-ray diffraction (XRD), scanning electron microscopy (SEM), and electron dispersive spectroscopy (EDS) analyses were performed before the ASTM G1[25] procedure was followed to remove the corrosion products and determine the corrosion rate by weight loss. Surface profile analysis then was performed to investigate the extent of localized corrosion.

RESULTS

Large-Scale Flow Loop

Pictures of the weight-loss samples taken immediately after the end of the test and after removal of the corrosion product layer are shown in Figure 3 (Test 1) and Figure 4 (Test 2). SEM/EDS analyses are also presented. The morphology of the corrosion product layer was quite varied, from very small crystallites seen in Test 1 (at low WCR) to a more amorphous layer seen in Test 2 (at higher WCR). The presence of FeS was identified in both tests as expected, although no phase identification could be performed.

Once the corrosion product layer was removed, the steel surface looked fairly uniform with only sparse traces of localized corrosion, with isolated pits ranging from 80 μm to 130 μm in depth. The maximum pitting rate then was calculated at 1.3 mm/y for Test 1 and 2.7 mm/y for Test 2. However, it should be mentioned that the percentage of the coupon surface affected by localized corrosion was very small in both tests. The pits could not be found with simple visual inspection and required the use of a surface profilometer to be identified.

Figure 5 shows the general corrosion rate results obtained in the two large-scale flow loop tests. The number above each data point represents the number

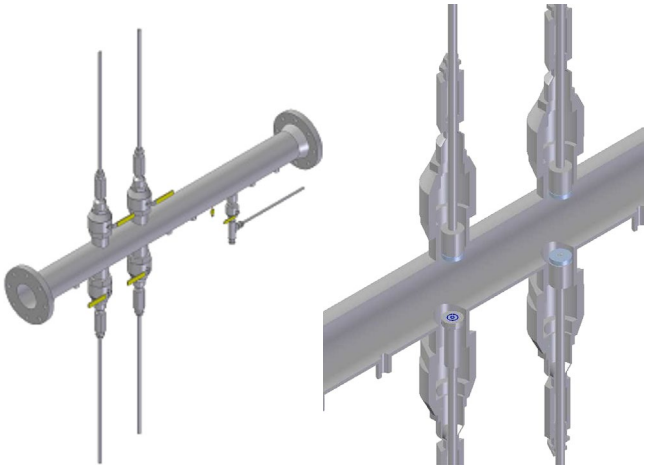

(a) Full view (b) Cross-sectional view

FIGURE 1. *Schematic of the UNS N10276 flow loop TLC test section.*

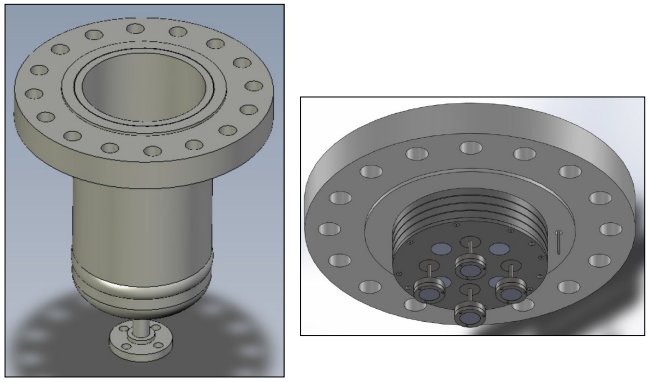

FIGURE 2. *The (left) 20 L UNS N10276 autoclave setup and (right) details of the cooled sample holder.*

(a) Sample with intact corrosion product layer

(b) Sample after removal of the corrosion layer

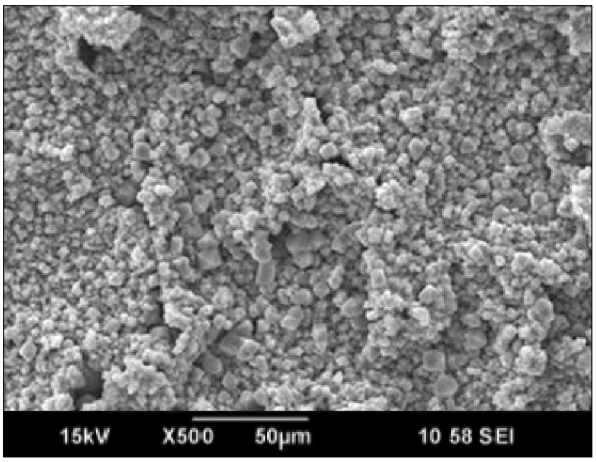

(c) SEM of the corrosion product layer X500

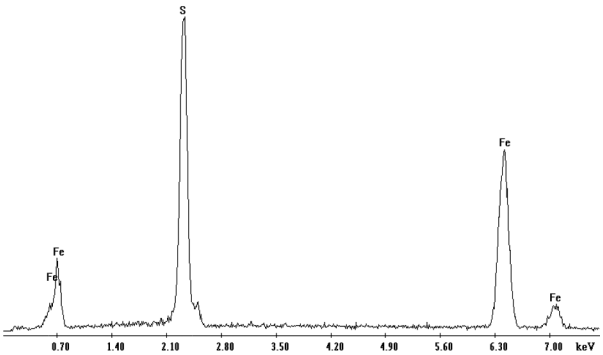

(d) EDS analysis of the corrosion product layer seen in (c)

FIGURE 3. *Analysis of the corrosion product layer. Flow loop test 1, top of the line, test duration: 19 days.*

of weight-loss samples used to calculate the average TLC rate, and the error bar corresponds to the maximum and minimum TLC rates measured.

In Test 2, the concentration of undissociated acetic acid was slightly higher than in Test 1 (upon request by the sponsor of the study). The results seem to show that the WCR had little to no effect on the general corrosion rate. This is contrary to sweet, CO_2-dominated TLC, where the condensation rate has a definite influence on the corrosion rate. Although any explanation at this stage is tentative, it can be inferred that since FeS does not need significant bulk supersaturation to form on the steel surface (as opposed to $FeCO_3$), the amount of water condensing should not matter as much as it does in CO_2-dominated TLC. This does not mean, however, that the condensation has no effect. The presence of water condensing on the steel sample is still essential for the corrosion reactions to happen.

Autoclave

This section presents in detail the results obtained with the 20 L autoclave. The objective of Test 3 was to build a link between the large flow loop and the autoclave tests, as similar conditions were used. Tests 4 through 7 focused on simulating the Karan field conditions more closely.

Test 3: Comparison Between Flow Loop and Autoclave Results — Although the conditions were not exactly identical (T_{gas}: 40°C instead of 55°C for the flow loop tests), the flow loop and autoclave results were similar enough to make a comparison. Results of the autoclave test are shown in Figure 6. The TLC rate showed good repeatability and agreed rather well with the flow loop results (0.3 mm/y for the autoclave compared to 0.2 mm/y to 0.4 mm/y for the flow loop over a 3 week period), giving encouraging evidence that autoclave tests should be able to produce reliable TLC data. The corrosion product analysis shows the presence of a porous superficial layer identified as an iron sulfide (most likely mackinawite, although no XRD analysis was performed). The sample was uniformly corroded and no trace of localized corrosion could be found during the surface profile analysis (not shown here).

Tests 4 through 7: Influence of High Partial Pressure of H_2S on Top-of-the-Line Corrosion — Photographs of the weight-loss samples taken immediately

(a) Sample with intact corrosion product layer

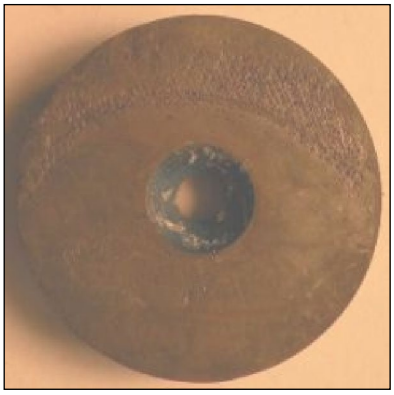

(b) Sample after removal of the layer

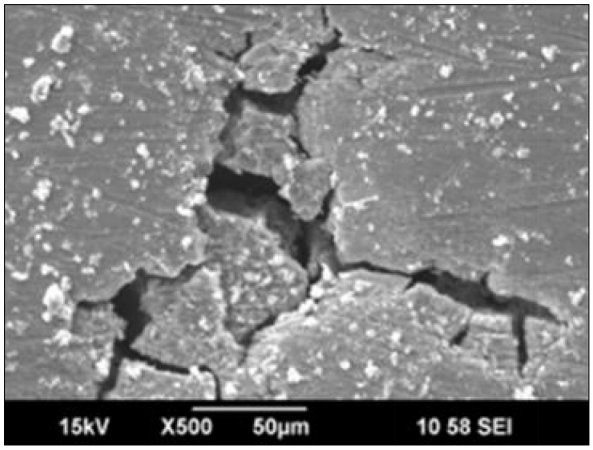

(c) SEM of the corrosion product layer X500

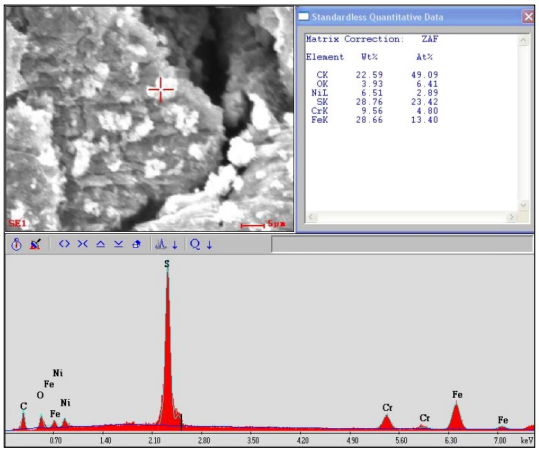

(d) EDS analysis of the corrosion product layer seen in (c)

FIGURE 4. *Analysis of the corrosion product layer. Flow loop test 2, top of the line, duration: 22 days.*

after the end of the test are shown in Figure 7. The steel samples had very similar appearances, with a gray layer covering the entire surface. Rounded markings were visible and were indications of the presence of droplets of condensed water, typically 10 mm to 12 mm diameter, on the surface of the steel samples. No clear indication of breakdowns in the corrosion product layer could be observed.

Unusual features could be observed by SEM, all apparently forms of FeS, as suggested by the EDS elemental analysis (Figure 8). The variety of the morphologies observed potentially implies that different phases of FeS formed on the steel surface. The corresponding XRD analysis of the corrosion product layer shows the presence, depending on the test conditions, of troilite, mackinawite, and cubic FeS. The standard line intensities of these FeS phases are shown for comparison in Figure 9. The works of Smith and coworkers[26-28] are helpful in providing explanations for the occurrence of different iron sulfide corrosion products. Figure 10 also represents the domain of stability of each stable FeS phase.

At low to moderate temperatures, mackinawite is favored usually in short-term exposures, because

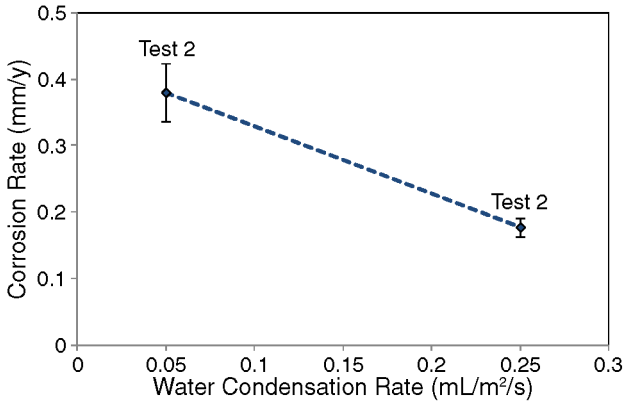

FIGURE 5. *TLC rate comparison between results from Test 1 (undissociated HAc = 250 mg/L, WCR = 0.25 mL/m²/s) and Test 2 (undissociated HAc = 350 mg/L, WCR = 0.05 mL/m²/s).*

the kinetics of mackinawite formation are faster than any other FeS species.[29] Mackinawite has been identified as the main FeS phase in every experiment performed. Cubic FeS is the least stable of the three FeS phases and, consequently, is favored by a high saturation level (i.e., high concentration of Fe^{2+} ions) and

(a) Steel sample with corrosion product layer

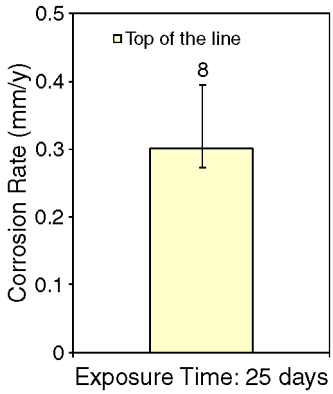

(b) Top of line corrosion rate

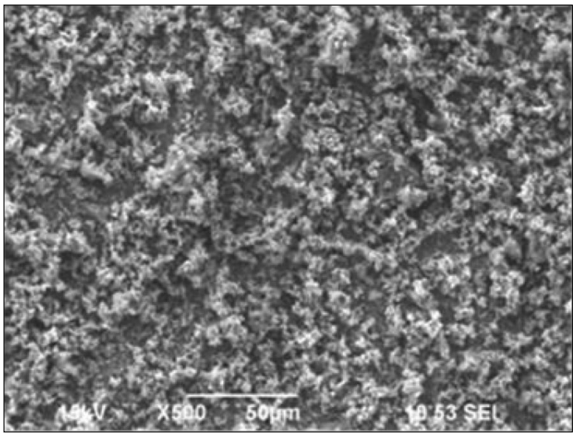

(c) SEM of the corrosion product layer X500

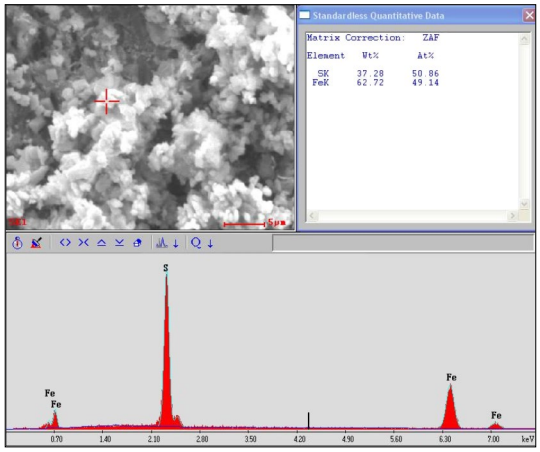

(d) EDS analysis of the corrosion product layer seen in (c)

FIGURE 6. *Analysis of the corrosion product layer. Autoclave test 3, top of the line, exposure time: 25 days.*

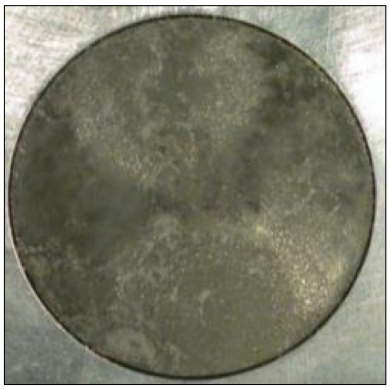

(a) Steel sample from Test 5 with corrosion product layer

(b) Steel sample from Test 6 without corrosion product layer

FIGURE 7. *Weight loss (WL) coupons before the removal of the corrosion product. Autoclave tests 5 and 6, top of the line, exposure time: 21 days.*

low temperature (between 35°C and 50°C).[29] A condensed water environment is also ideal for its formation since it is inhibited by the presence of "foreign ions" such as Cl^- ions.[30] It, however, should transition quickly into more stable pyrrhotite or mackinawite.[31] Troilite has been observed in top-of-the-line scenarios before[15] with characteristic needle-shaped crystals. Troilite is a stochiometric form of pyrrhotite, which is favored in acidic solutions but is also kinetically slower than mackinawite.[30] Consequently, a combination of higher temperature, lower pH, and higher H_2S content should favor its formation.

For Test 4 (199 kPa of H_2S, T_{gas}: 45°C), XRD analysis identified the corrosion product layer as com-

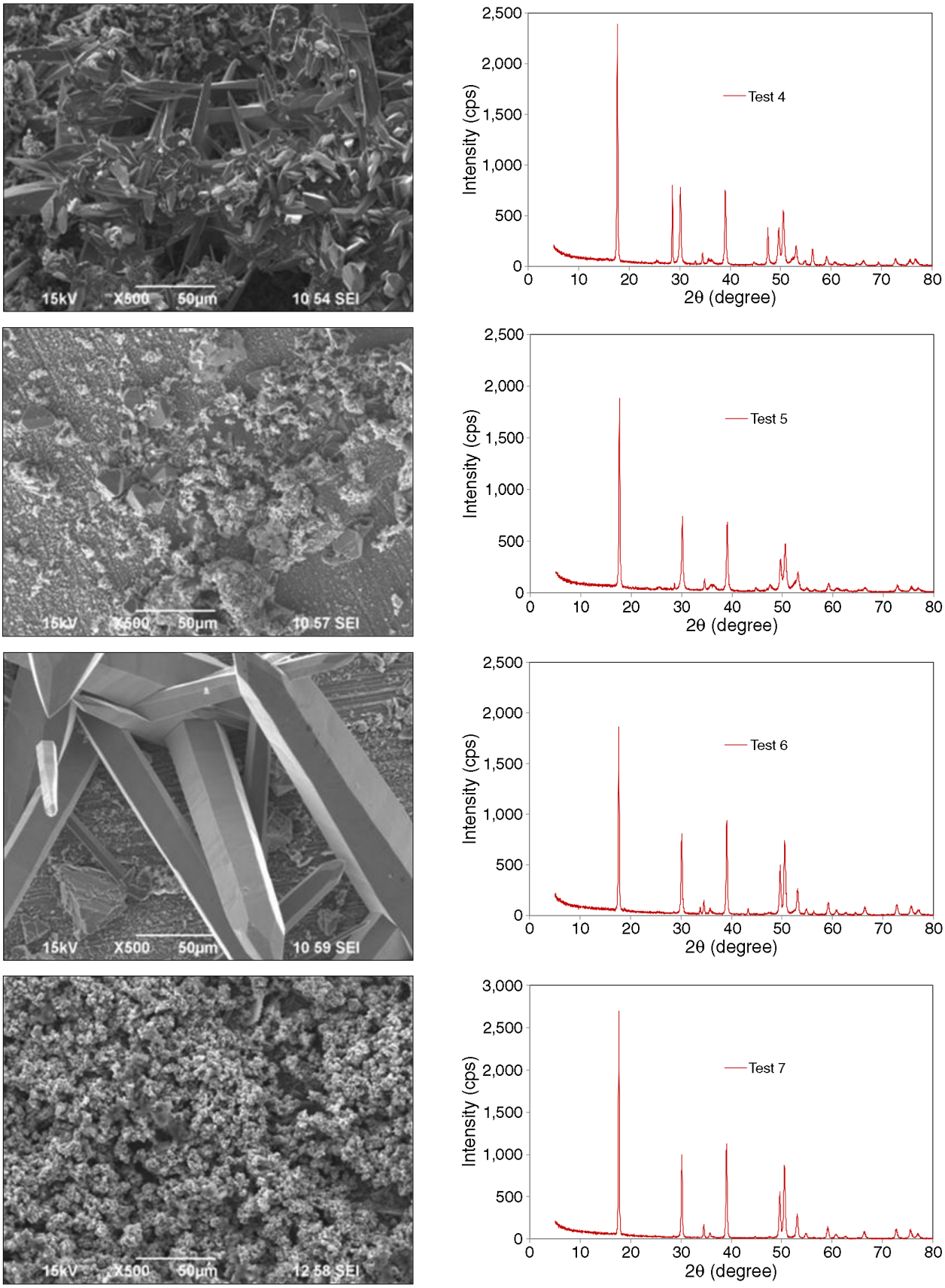

FIGURE 8. *SEM and XRD analyses of the corrosion product layer. Autoclave tests 4, 5, 6, 7, top of the line, exposure time: 21 days.*

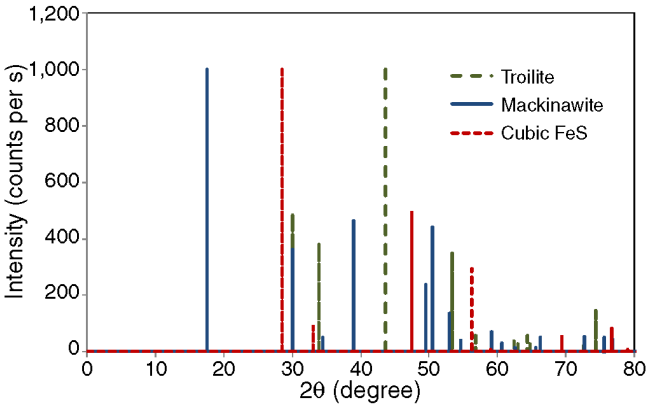

FIGURE 9. *XRD analysis – Standard pics for troilite, mackinawite, and cubic FeS.*

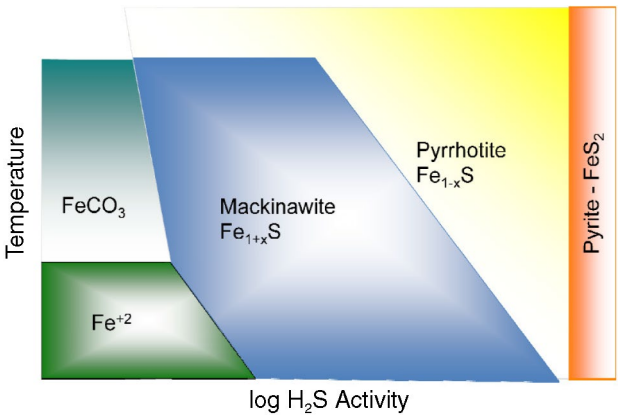

FIGURE 10. *Stability of Fe_xS_y products with regard to temperature and H_2S activity.*[26-28]

prising mackinawite and cubic FeS. Although the steel temperature was relatively high (38°C) as a result of the low water condensation rate, the H_2S content may not have been sufficient to trigger the formation of troilite.

Tests 5 and 7 were performed at higher condensation rates (0.12 mL/m^2/s and 0.14 mL/m^2/s), at two different H_2S partial pressures (124 kPa and 429 kPa, respectively) and at a higher gas temperature (T_{gas}: 55°C). The XRD/SEM analyses were quite similar to those reported above for Test 4. The presence of mackinawite was identified in both cases together with very small amounts of cubic FeS in Test 5 (pH_2S: 124 kPa). This could be explained by the lower sample temperature (as a result of high WCR), measured around 20°C to 25°C, which did not favor kinetically slow reactions (i.e., troilite).

For Test 6 (low WCR, T_{gas}: 55°C, pH_2S: 429 kPa), the XRD analysis performed on the coupon surface identified mackinawite and traces of troilite. In this case, lower condensation rates, higher steel temperature (50°C), and higher partial pressure of H_2S (429 kPa) logically facilitated the formation of troilite.

Cross-sectional analysis also was performed and the results are presented in Figures 11 through 14. For Test 4, the very dense and adherent FeS layer on the metal surface is 10 µm to 20 µm thick, while the steel lost an average of 13.7 µm as a result of corrosion. Therefore, there was a close match between the thickness of the lower portion of the adherent layer and the steel thickness loss. However, different locations of the cross section showed the presence of features above this dense layer, though no clear difference in chemical composition was found between the two. This outer layer of FeS probably corresponded to the larger features observed in other SEM images. Nevertheless, the overall roughness of the steel surface indicated that the corrosion attack was uniform.

For Test 5, the FeS layer also was composed of two parts: a dense and adherent layer covering the steel surface with an average thickness of just under 7 µm and a second, very porous layer on top of the previous one, with an average thickness of about 40 µm. By comparison, the steel thickness loss from corrosion was 4.5 µm, which corresponded roughly to the thickness of the first layer. The porosity of the second layer could be inferred by observing the SEM images. Since the outer layer was much thicker than the calculated "wall thickness loss," it most likely formed through a precipitation process. The EDS elemental analysis showed no significant chemical composition difference between the two types of layers, both identified as FeS. In addition, no localized corrosion could be observed on the bare steel surface once the layer was removed.

As observed in the two previous tests, the corrosion product layer for Test 6 seemed to be comprised of two distinct layers. A dense and seemingly adherent layer covered the steel surface with a thickness around 10 µm (which was significantly more than the average 4 µm wall loss). On top of this first layer, larger features corresponding to the "troilite needles" could be found, corresponding to the crystals observed in the SEM images. Both layers had a similar chemical composition. Once again, no localized corrosion could be found on the bare metal surface.

For Test 7, the corrosion product layer presented the same characteristics as those observed at higher condensation rates in Test 5. A thick and very porous layer covered a more dense and adherent inner film. The porous layer was about 25 µm to 30 µm thick, while the dense layer was on average only 10 µm thick. By comparison, the wall loss by corrosion was 7.5 µm. The small crystals "trapped" in the epoxy matrix seen in the cross-sectional images corresponded to those observed in the SEM images of the corrosion product layer surface. Once again, there were no chemical composition differences between the two layers and the corrosion attack was uniform. Although no surface profile analysis is shown, the metal surface of all the samples was always uniformly

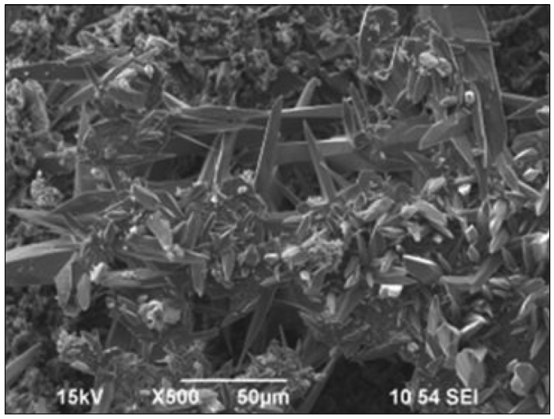

(a)SEM image of corrosion product layer X500

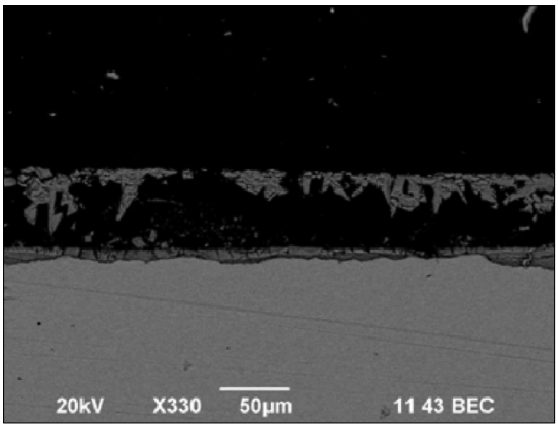

(b) Cross section of steel sample with corrosion product layer X330

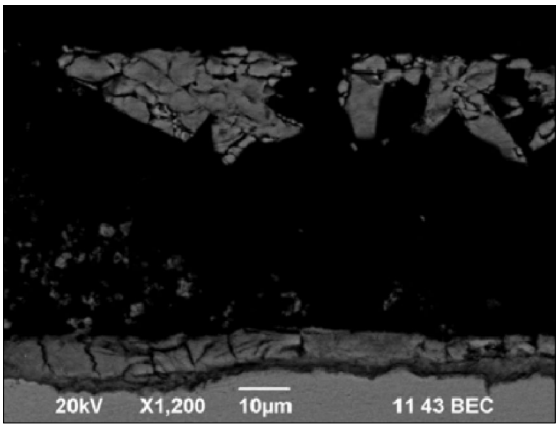

(c) Cross section of steel sample with corrosion product layer X1,200

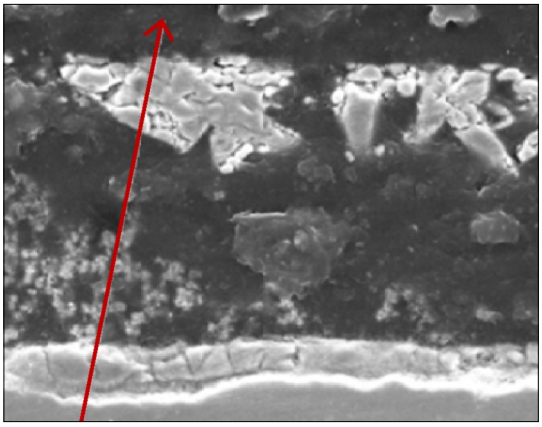

(d) Details of cross section of steel sample with corrosion product layer (arrow - EDS scan)

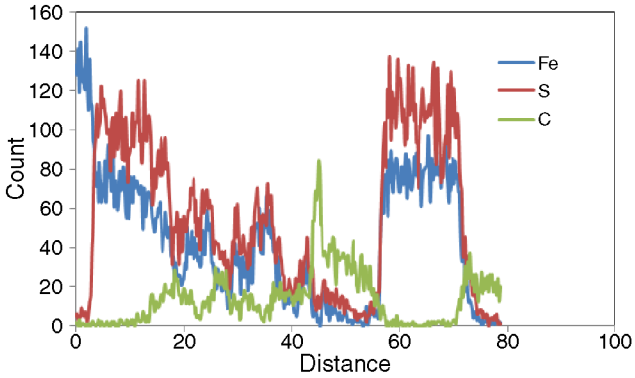

(e) EDS scan analysis along the arrow in the cross section of steel sample with corrosion product layer (see [d])

FIGURE 11. *Cross-sectional analysis of steel sample with corrosion product layer. Autoclave test 4, top of the line, duration 21 days.*

corroded and no trace of localized corrosion could be found.

Considering the differences in the kinetics of formation of mackinawite vs. cubic FeS or troilite/pyrrhotite, Smith, et al.,[26] proposed a two-step mechanism involving the rapid formation of a thin mackinawite layer on the metal surface "overlain" by potentially different phases of iron sulfide. This "two-step" mechanism seemed to be validated by the analysis of the cross section performed in this study. The growth rate of the first layer appeared to be related directly to the corrosion rate, since its thickness often corresponded to the uniform metal loss. The identity of the second phase depended more on the actual test conditions than on the kinetics of corrosion product formation. Low temperature (linked to higher conden-

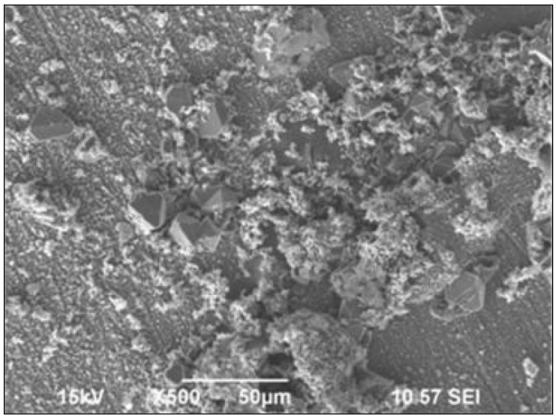

(a)SEM image of corrosion product layer X500

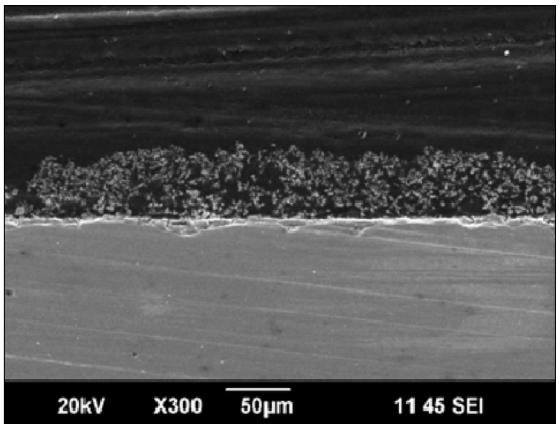

(b) Cross section of steel sample with corrosion product layer X300

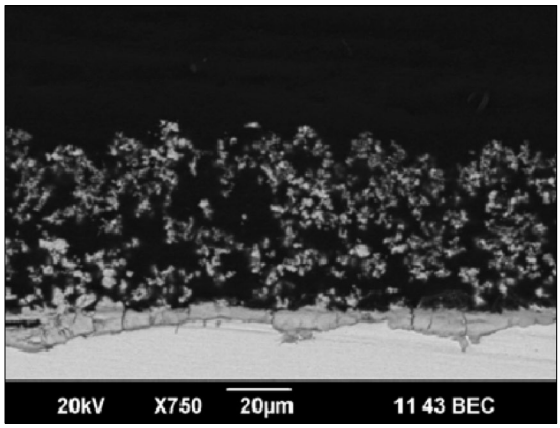

(c) Cross section of steel sample with corrosion product layer X750

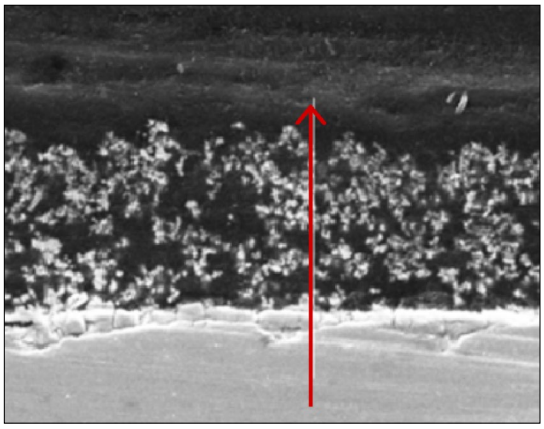

(d) Details of cross section of steel sample with corrosion product layer (arrow - EDS scan)

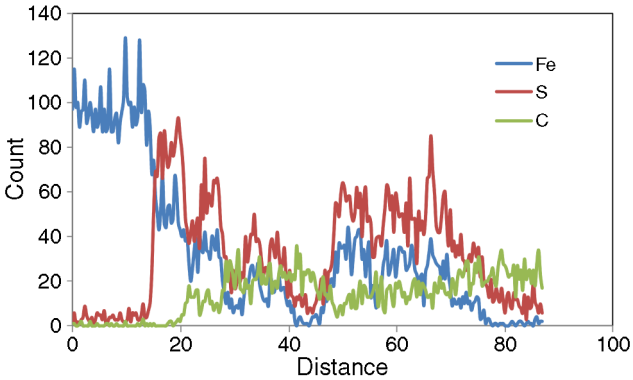

(e) EDS scan analysis along the arrow in the cross section of steel sample with corrosion product layer (see [d])

FIGURE 12. *Cross-sectional analysis of steel sample with corrosion product layer. Autoclave test 5, top of the line, duration 21 days.*

sation rate) seemed to favor the formation of a very porous mackinawite. At higher temperatures (45°C to 50°C), cubic FeS crystals could nucleate more rapidly. Higher temperature and higher H_2S partial pressure lead to the formation of troilite and probably pyrrhotite. The corrosion rates for each of the autoclave tests are shown in Figure 15, together with a summary of the most influential parameters (pH_2S, gas temperature, steel surface temperature, water condensation rate). It is not easy to compare the test results, because more than one parameter changed between experiments. An effort to isolate the influence of each parameter is discussed in the next section.

Figure 16 presents a comparison between the time-averaged flux of Fe^{2+} leaving the steel and the time-averaged flux of Fe^{2+} consumed for the FeS scale

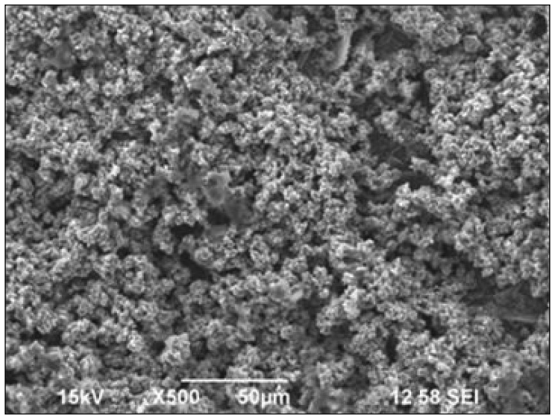

(a)SEM image of corrosion product layer X500

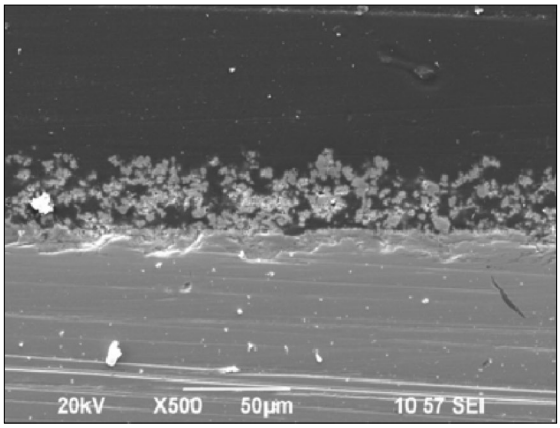

(b) Cross section of steel sample with corrosion product layer X500

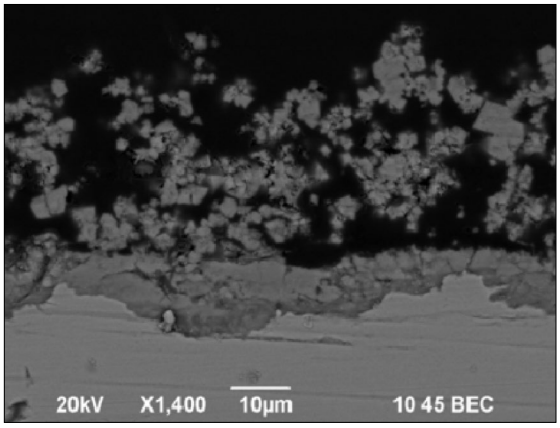

(c) Cross section of steel sample with corrosion product layer X1,400

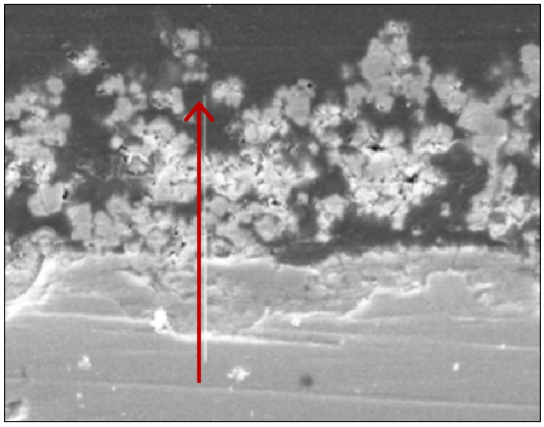

(d) Details of cross section of steel sample with corrosion product layer (arrow - EDS scan)

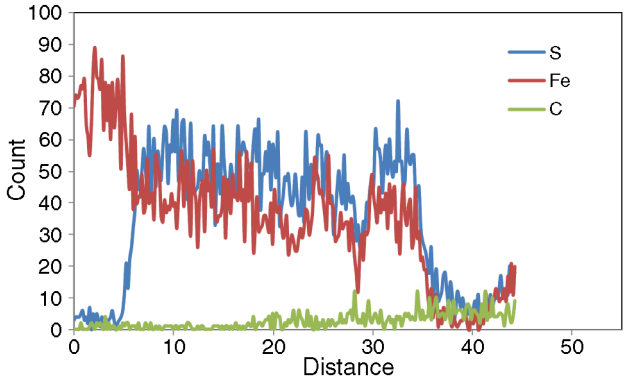

(e) EDS scan analysis along the arrow in the cross section of steel sample with corrosion product layer (see [d])

FIGURE 13: *Cross-sectional analysis of steel sample with corrosion product layer. Autoclave test 7, top of the line, duration 21 days.*

formation. Using the same unit of $mol_{Fe^{2+}}/m^2/s$, the steel dissolution rate (corrosion rate) and the scale formation rate (formation rate of FeS) can be compared.

In all cases, the layer is assumed to be made entirely of mackinawite. This graph helps evaluate how much of the iron dissolved by corrosion ends up being used in the layer formation process. In this TLC scenario, the Fe^{2+} ions present in the condensed water can come only from the corrosion process happening in situ, since there is no bulk solution like there is at the bottom of the line. Consequently, the scale formation rate always should be lower or equal to the steel dissolution rate. Often, about half of all the Fe^{2+} ions released through corrosion are used for the FeS layer formation, although there is a scatter in the results.

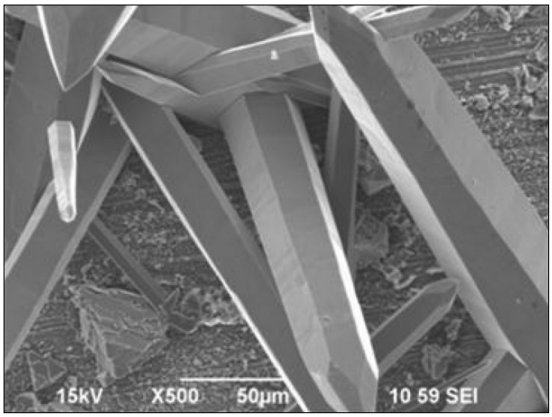

(a)SEM image of corrosion product layer X500

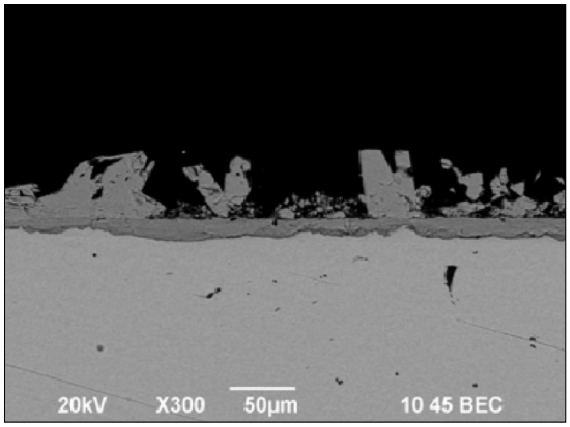

(b) Cross section of steel sample with corrosion product layer X300

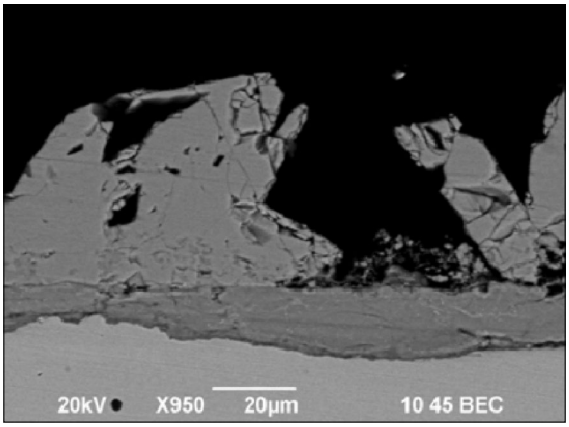

(c) Cross section of steel sample with corrosion product layer X950

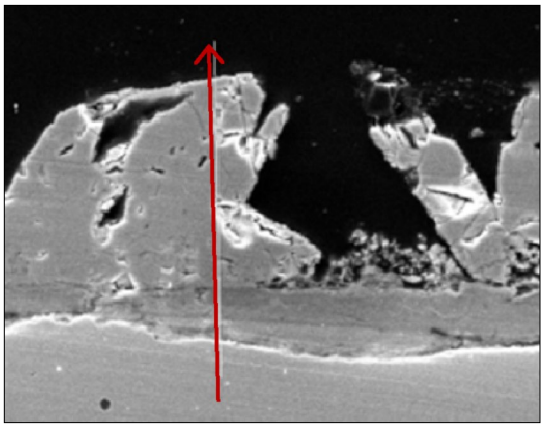

(d) Details of cross section of steel sample with corrosion product layer (arrow - EDS scan)

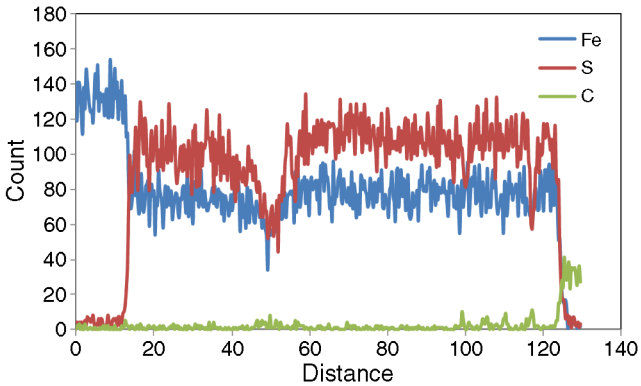

(e) EDS scan analysis along the arrow in the cross section of steel sample with corrosion product layer (see [d])

FIGURE 14. *Cross-sectional analysis of steel sample with corrosion product layer. Autoclave test 6, top of the line, duration 21 days.*

The results obtained through Test 6 show, however, the opposite behavior with a scale formation rate being higher than the steel dissolution rate. This discrepancy has not been explained to date and could be because of errors related to the trapping of water within formed corrosion product layers, iron sulfide oxidation by atmospheric O_2 during sample recovery, or through balance error.

DISCUSSION

The influence of the main parameters on the average corrosion rate are discussed, drawing from experimental data in Tables 3 and 4. However, it should be understood that many conditions changed between the tests (temperature, pH_2S, and condensation rate) and that comparisons cannot be made directly.

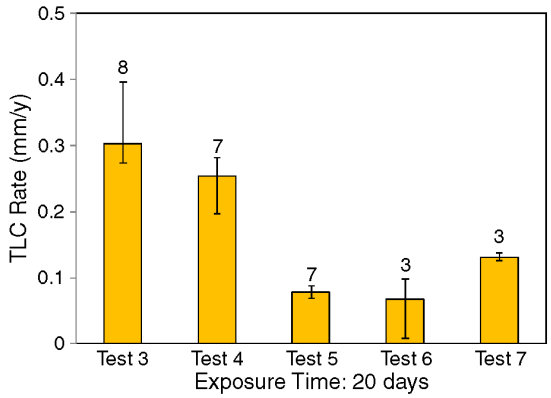

pH_2S / (kPa):	11	199	124	429	429
WCR/ (mL/m^2/s):	0.14	0.02	0.12	0.02	0.14
T_{gas} / (°C):	40	45	55	55	55
$T_{steel\ surface}$ / (°C):	17	38.1	21.4	50	24.4
pCO_2 / (kPa)	41	813	940	990	990

FIGURE 15. *Autoclave tests, corrosion rate analysis. Top of the line, exposure time: 21 days.*

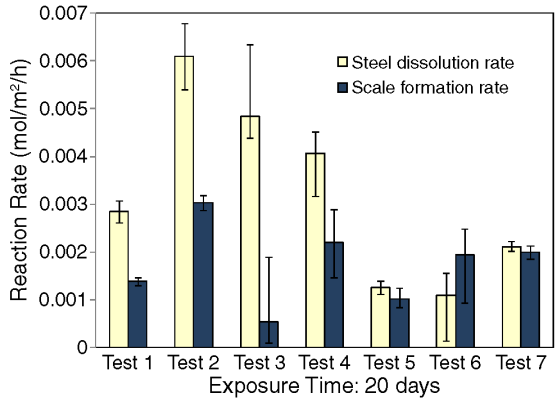

pH_2S / (kPa):	10	10	11	199	124	429	429
WCR / (mL/m^2/s):	0.25	0.05	0.14	0.02	0.12	0.02	0.14
T_{gas} / (°C):	55	55	40	45	55	55	55
$T_{steel\ surface}$ / (°C):	~25	~50	17	38.1	21.4	50	24.4
pCO_2 / (kPa)	50	50	41	810	940	990	990

FIGURE 16. *Comparison between scale formation rate and steel dissolution rate. Top of the line, exposure time: 21 days.*

TABLE 4
Tests 3 through 7—Large-Scale (20 L) Autoclave—Experimental Results

	Test 3	Test 4	Test 5	Test 6	Test 7
Average CR (mm/y)	0.3	0.25	0.08	0.07	0.13
Max. (mm/y)	0.09	0.03	0.01	0.03	0.01
Min. (mm/y)	0.03	0.06	0.01	0.06	0.01

The effect of the condensation rate is analyzed first. As in CO_2-dominated TLC, condensation has a primary influence. In that case (sweet systems), low condensation rates lead to high pH and high supersaturation with respect to $FeCO_3$ inside the droplets. A protective layer forms and the corrosion remains low. If the condensation rate is higher (critical value of 0.25 mL/m^2/s or 0.025 mL/m^2/s have been proposed[32]), sufficient saturation levels ensuring $FeCO_3$ stability cannot be achieved and high general or localized corrosion rates are experienced. In sour systems, the FeS layer is fairly insoluble in water and FeS formation occurs almost instantaneously at the metal surface. Under these conditions, it is believed that the pH in the condensed water always remains quite low, and the effect of the condensation rate is minimized.[15] This is what is seen in Tables 3 and 4, where the influence of the condensation is not present. Other authors have made similar observations, finding the influence of condensation to be secondary and stressing the importance of the iron sulfide scale characteristics.[17] That said, if Tests 6 and 7 are directly compared, a tenfold increase in the condensation rate (from 0.02 mL/m^2/s to 0.14 mL/m^2/s) led to a doubling of the corrosion rate (from 0.07 mm/y to 0.12 mm/y). However, this effect is believed to be overcome by other parameters, such as the temperature.

Looking at the effect of the partial pressure of H_2S or the CO_2/H_2S ratio, no correlation with corrosion behavior was apparent. Higher partial pressure of H_2S should lead to a more aggressive environment; however, this produces more protective FeS scale. Field experience on that matter is also inconclusive, with strictly no indication of TLC in onshore/offshore pipelines subjected to a wide range of CO_2/H_2S ratio (2% to 17% H_2S and 3% to 10% CO_2).[21]

Figure 17 shows the influence of the gas temperature and an apparent correlation with the corrosion rate. Higher corrosion rates have been reported at lower temperatures,[17] and the same is true for the experiments in this study. However, the corrosion reaction, including layer formation, should be controlled by the temperature at which it occurs, i.e., the steel temperature instead of the gas temperature, which can be quite different. Tables 3 and 4 present the corresponding average corrosion rate and steel surface temperature (which is calculated based on the in-house condensation rate model described earlier) obtained for each test. No correlation could be seen here, which was unexpected. One could question the validity of the temperature predictions, but this is unlikely since their accuracy has been validated against controlled laboratory environments.[24] The other possibility is that the overall process is controlled by the liquid/vapor equilibrium reactions, which depend more on the gas temperature.

Finally, considering the results available from the XRD analyses (Tests 4 through 7), the highest corro-

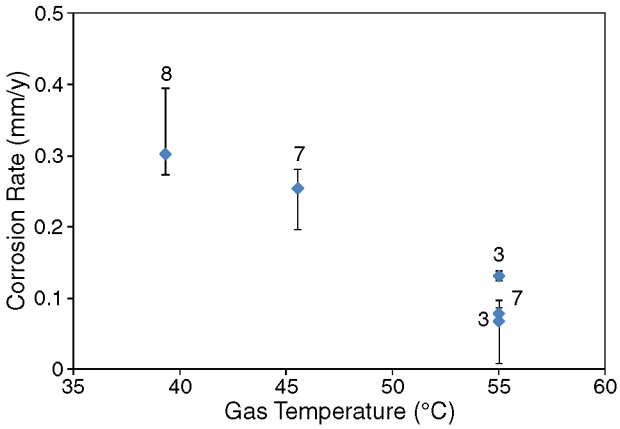

FIGURE 17. *Influence of the gas temperature on TLC.*

sion rate was measured when a mixture of cubic FeS and mackinawite was detected on the steel surface. Pure mackinawite seemed to lead to general attack and to a lower corrosion rate. Further work is needed in this area.

CONCLUSIONS

❖ The 20 L autoclave seemed to produce more reliable data as compared to the large-scale (2,000 L), multiphase flow loop tests. It also enabled a more representative simulation of the field conditions with regard to the high H_2S partial pressure.

❖ The experiments conducted here in sour conditions resulted in relatively low average corrosion rates under water condensing conditions (below 0.5 mm/y) in both flow loop and autoclave tests.

❖ One instance of localized corrosion was observed in a flow loop test (pitting rate of 2.7 mm/y after 21 days of testing).

❖ The corrosion attack seemed to be controlled mainly by the gas temperature (lower temperature leading to higher corrosion rate). The protective properties of the FeS layer seemed to play a key role. Mackinawite, cubic FeS, and troilite were identified using XRD in the corrosion product layer. The condensation rate, partial pressure of H_2S, or H_2S/CO_2 ratio did not seem to have a clear influence on the corrosion rate.

REFERENCES

1. R. Paillassa, M. Dieumegard, M. Estevoyer, "Corrosion Control in the Gathering System at Lacq Sour Gas Field," in Proc. 2nd Int. Congress of Metallic Corrosion (New York, 1963), p. 410-417.
2. Y. Gunaltun, D. Supriyataman, J. Achmad, *Oil Gas J.* 97, 28 (1999): p. 64.
3. M. Thammachart, Y. Gunaltun, S. Punpruk, "The Use of Inspection Results for the Evaluation of Batch Treatment Efficiency and the Remaining Life of the Pipelines Subjected to Top of Line Corrosion," CORROSION/2008, paper no. 08471 (Houston, TX: NACE International, 2008).
4. D.F. Ho-Chung-Qui, A.I. Williamson, P. Eng, "Corrosion Experiences and Inhibition Practices in Wet Sour Gathering Systems," CORROSION/1987, paper no. 46 (Houston, TX: NACE, 1987).
5. N.N. Bich, K.E. Szklarz, "Crossfield Corrosion Experience," CORROSION/1988, paper no. 196 (Houston, TX: NACE, 1988).
6. R.L. Martin, *Mater. Perform.* 48, 12 (2009): p. 48-52.
7. M. Edwards, B. Cramer, "Top of the Line Corrosion—Diagnostic, Root Cause Analysis and Treatment," CORROSION/2000, paper no. 72 (Houston, TX: NACE, 2000).
8. M. Joosten, D. Owens, A. Hobbins, H. Sun, M. Achour, D. Lanktree, "Top-of-Line Corrosion—A Field Failure," paper 9524, Proc. EuroCorr (Moscow, Russia, 2010).
9. M. Singer, S. Nešić, Y. Gunaltun, "Top of the Line Corrosion in Presence of Acetic Acid and Carbon Dioxide," CORROSION/2004, paper no. 4377 (Houston, TX: NACE, 2004).
10. C. Mendez, M. Singer, A. Camacho, S. Hernandez, S. Nešić, "Effect of Acetic Acid, pH and MEG on CO_2 Top of the Line Corrosion," CORROSION/2005, paper no. 5278 (Houston, TX: NACE, 2005).
11. T. Andersen, A.M.K. Halvorsen, A. Valle, G. Kojen, "The Influence of Condensation Rate and Acetic Acid Concentration on TOL Corrosion in Multiphase Pipelines," CORROSION/2007, paper no. 7312 (Houston, TX: NACE, 2007).
12. R. Nyborg, A. Dugstad, "Top of the Line Corrosion and Water Condensation Rates in Wet Gas Pipelines," CORROSION/2007, paper no. 7555 (Houston, TX: NACE, 2007).
13. D. Hinkson, M. Singer, Z. Zhang, S. Nešić, *Corrosion* 66, 6 (2010): p. 045002.
14. M. Singer, D. Hinkson, Z. Zhang, H. Wang, S. Nešić, "CO_2 Top of the Line Corrosion in Presence of Acetic Acid—A Parametric Study," CORROSION/2009, paper no. 9292 (Houston, TX: NACE, 2009).
15. M. Singer, A. Camacho, B. Brown, S. Nešić, *Corrosion* 67, 8 (2011): p. 085033.
16. R. Nyborg, A. Dugstad, T. Martin, "Top of Line Corrosion with High CO_2 and Traces of H_2S," CORROSION/2009, paper no. 9283 (Houston, TX: NACE, 2009).
17. D.V. Pugh, S.L. Asher, J. Cai, W.J. Sisak, "Top-of-Line Corrosion Mechanism for Sour Wet Gas Pipelines," CORROSION/2009, paper no. 9285 (Houston, TX: NACE,).
18. J. Kvarekval, "The Influence of Small Amounts of H_2S on CO_2 Corrosion of Iron and Carbon Steel," in Proc. Eurocorr (Gloshavgen, Norway: NTNU, 1997).
19. A. Valdes, R. Case, M. Ramirez, A. Ruiz, "The Effect of Small Amounts of H_2S on CO_2 Corrosion of Carbon Steel," CORROSION/1998, paper no. 22 (Houston, TX: NACE, 1998).
20. B. Brown, K.L. Lee, S. Nešić, "Corrosion in Multiphase Flow Containing Small Amounts of H_2S," CORROSION/2003, paper no. 3341 (Houston, TX: NACE, 2003).
21. M. Bonis, "Form Sweet to Sour TLC: What's Different?," 2nd Int. TLC Conf. (Houston, TX: NACE, 2009).
22. S. Smith, M. Joosten, "Corrosion of Carbon Steel by H_2S in CO_2 Containing Environments," CORROSION/2006, paper no. 6115 (Houston, TX: NACE, 2006).
23. M. Singer, B. Brown, A. Camacho, S. Nešić, *Corrosion* 67, 1 (2011): p. 015004.
24. Zhang, D. Hinkson, M. Singer, H. Wang, S. Nešić, *Corrosion* 63, 11 (2007): p. 1051-1062.
25. ASTM G1, "Standard Practice for Preparing, Cleaning, and Evaluating Corrosion Test Specimens" (West Conshohocken, PA: ASTM International, 2003).
26. S. Smith, B. Brown, W. Sun, "Corrosion at Higher H_2S Concentrations and Moderate Temperatures," CORROSION/2011, paper no. 11081 (Houston, TX: NACE, 2011).
27. S. Smith, E.J. Wright, "Prediction of Minimum H_2S Levels Required for Slightly Sour Corrosion," CORROSION/1994, paper no. 11 (Houston, TX: NACE, 1994).
28. S. Smith, "A Proposed Mechanism for Corrosion in Slightly Sour Oil and Gas Production," in Proc. Int. Corrosion Congress, paper 385 (Australiasian Corrosion Association, 1993).
29. D.W. Shoesmith, P. Taylor, M.G. Bailey, D.G. Owen, *J. Electrochem. Soc.* 127, 5 (1980): p. 1007-10015.
30. R.D. Medicis, *Science* 170, 3963 (1970): p. 1191-1192.
31. J.B. Murowchick, H.L. Barnes, *Am. Mineral.* 71 (1986): p. 1243-1246.
32. Y. Gunaltun, R. Piccardino, D. Vinazza, "Interpretation of MFL and UT Inspection Results in Case of Top of Line Corrosion," CORROSION/2006, paper no. 6170 (Houston, TX: NACE, 2006).